Supplemental Data

Neuregulin1/ErbB4 Signaling Induces

Cardiomyocyte Proliferation and

Repair of Heart Injury

Kevin Bersell, Shima Arab, Bernhard Haring, and Bernhard Kühn

Supplemental Data for this manuscript include:

Supplemental Experimental Procedures

Figures and Legends S1–S7

Tables S1–S8

Supplemental References

Supplemental Experimental Procedures

Mouse strains

ErbB4$^{F/F}$ mice were obtained from the NIH-sponsored Mutant Mouse Repository at University of California Davis and were originally produced by Dr. Kent Lloyd (Golub et al., 2004). The *α-MHC-MerCreMer* mice were obtained from the Jackson Laboratories and originally generated by Dr. Jeffrey Molkentin (Sohal et al., 2001). The *α-MCH-ErbB4* mice, originally generated by Dr. Martin Gassmann (Tidcombe et al., 2003), were obtained from Dr. Gabriel Corfas (Children's Hospital Boston). The *Rosa26lacZ* mice were obtained from Jackson Laboratories and originally produced by Dr. Phillippe Soriano (Soriano, 1999). All mice were crossed to C57Bl/6 mice purchased from Taconic Laboratories. The Children's Hospital Institutional Animal Care and Use Committee approved all of the animal experiments.

Determination of recombination

To determine deletion of *ErbB4* exon 2 at the genomic level, we performed PCR on genomic DNA prepared from myocardium as described (Jackson-Fisher et al., 2006). Tamoxifen-injected, but not oil-injected *α-MHC-MerCreMer$^{+/+}$*; *ErbB4$^{F/F}$* mice had a 507 bp PCR product indicating high specificity of the deletion system. Expression of ErbB4 protein, detected with an antibody provided by Cary Lai (#0616, Salk Institute) and visualized by immunofluorescence microscopy, was decreased in cardiomyocytes isolated from test mice. To determine the efficiency of our deletion protocol, we crossed the *α-MHC-MerCreMer* allele into a *Rosa26lacZ* background (Soriano, 1999) and quantified the number of β-galactosidase-positive cardiomyocytes after injection of tamoxifen. We detected β-galactosidase activity in $83.5 \pm 2\%$ of cardiomyocytes ($n =$ 7) dispersed throughout the myocardium and no β-galactosidase activity in the absence of Cre (**Supplemental Figure S2C**). In conclusion, our inducible deletion strategy was very efficient

and highly specific for differentiated cardiomyocytes. Injection of Tamoxifen in *α-MHC-MerCreMer$^{+/+}$* did not affect cardiomyocyte cell cycle activity (**Supplemental Figure S2D**).

Determination of cardiomyocyte volumes and dimensions

Cardiomyocytes were isolated following Langendorff perfusion with collagenase II (20 mg/mL, Invitrogen) and protease XIV (2 mg/mL, Sigma). Contractile elements were visualized with immunofluorescent staining with an antibody against Troponin I (1:500, Santa Cruz Biotechnology). Invitrogen provided secondary antibodies raised in goat conjugated to Alexa594. Optical sections were obtained using laser scanning confocal microscopy (Olympus FV1000) with a step size of 0.5 μm. The images were digitally analyzed using Metamorph software to derive the cardiomyocyte volume. Cardiomyocyte width and length measurements were made on maximal intensity projections of these confocal stacks. Cardiomyocyte width was measured in 3 random locations and length was measured in the largest dimension parallel to the longitudinal axis.

Cardiomyocyte cross-sectional area

Horizontal cryosections of 14 μm thickness were stained with Masson's Trichrome. Images (×40 magnification) were analyzed using Metamorph software (Molecular Devices) to determine cross-sectional area.

Sarcomere disassembly

Horizontal cryosections of 14 μm thickness were stained with either α-actinin (1:100, Sigma) or myomesin (1:1,000, Developmental Studies Hybridoma Bank) antibodies to visualize Z-disk or M-band, respectively. Karyokinesis was visualized with a phosphorylated histone H3 antibody

3

(1:100, Upstate). Cytokinesis was visualized with an antibody against auroraB kinase, a required component of the contractile ring (1:500, Sigma). Images were obtained using a spinning-disk confocal microscope (DSU, Olympus).

Quantification of myocardial regeneration

We visualized myocardium and scar by AFOG staining (Kuhn et al., 2007). We determined myocardial volume and scar volume on ×1.5 magnification pictures by point count of pink and blue regions of tissue, respectively. We derived the volume per heart by quantifying 5–6 sections, spaced at 1 mm intervals. Cardiomyocyte nuclei were counted using the optical dissector method (Howard and Reed, 2005) on troponin I and DAPI-stained sections in 9 random sample volumes per heart. BrdU-positive cardiomyocyte nuclei were quantified on 3–5 sections per heart. Cardiomyocyte apoptosis was determined using the ApopTag Red In Situ apoptosis detection kit (Chemicon). We excluded the right ventricular free wall from the analysis.

Echocardiography

Sedation was induced in an environmental chamber with 3% isofluorane and maintained with 1% isofluorane delivered via nose cone mask. Echocardiography data were obtained using a Vivid*i* ultrasound device with a 12.5 MHz probe for **Supplemental Table S1** and using a VisualSonics device with a 40 MHz probe for **Figure 6B** and **Supplemental Tables S4** and **S5**.

Analysis of genetically labelled cardiomyocyte clusters

We treated *α-MHC-MerCreMer*$^{+/+}$*; Rosa26R*$^{+/-}$ mice with tamoxifen (5 µg/gm i.p. × 1) at postnatal age 15 days to induce site-specific recombination, leading to sparse labeling of differentiated cardiomyocytes. This labelling protocol resulted in $1.6 \pm 0.5\%$ X-gal-positive

cardiomyocytes. Five days later, NRG1 and BSA injections were given daily for 9 days. We prepared 14 μm cryosections, fixed them in 70% ethanol for 15 min, and developed X-gal staining by incubating in 1 mg/mL 5-bromo-4-chloro-3-indolyl-β-D-galactopyranoside for 12–48 hr. We performed clonal analysis by quantifying at least 200–400 X-gal positive cardiomyocyte clusters on at least two different sections per heart. The genetic labelling frequency was not different between NRG1- and BSA-injected animals (**Supplemental Figure S4B**). Furthermore, there was no correlation between variations of genetic labelling efficiency and the percentage of multicellular clusters of cardiomyocytes (**Supplemental Figure S4C**).

Analysis of contribution of stem cells

Using tamoxifen-induced site-specific recombination in the *α-MHC-MerCreMer$^{+/-}$; Rosa26R$^{+/-}$* strain, we reproducibly labeled 83.5 ± 2 % (*n* = 7) of differentiated cardiomyocytes with a permanent genetic tag (**Figure S2C**). Cell cycle activity in genetically unlabeled cardiomyocytes may be the result of an NRG1-effect on undifferentiated cardiac stem or progenitor cells. However, cell cycle activity in the tagged and untagged population of cardiomyocytes was the same, suggesting that undifferentiated stem or progenitor cells did not contribute to NRG1-induced cardiomyocyte cycling. If NRG1-induced cardiomyocyte cell cycle activity originated from differentiated cardiomyocytes, the genetic labeling efficiency should not influence the proliferative rate. Accordingly, the proliferative rate should be identical in genetically labeled and unlabeled cardiomyocytes irrespective of the percentage of genetically labeled cardiomyocytes. In contrast, if the NRG1-induced cardiomyocyte cell cycle activity in the genetically unlabelled population were derived from undifferentiated stem or progenitor cells, the genetic labeling efficiency should influence the proliferative rate. Accordingly, the proliferative rate should change with the percentage of genetically labeled cardiomyocytes. To address these possibilities, we modified our protocol such that we genetically labeled decreasing proportions of differentiated cardiomyocytes. The proliferative rate was the same at low,

intermediate, and high genetically labeled proportions of differentiated cardiomyocytes (**Figure 5D**). Thus, the proportion of cycling cardiomyocytes was not a function of the labeling efficiency. In conclusion, NRG1-induced cardiomyocyte cell cycle activity did not originate from undifferentiated stem or progenitor cells.
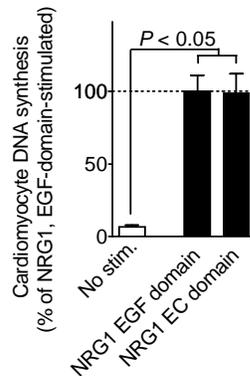
Supplemental Figure and Legend S1

Figure S1. The epidermal growth factor-like domain of NRG1 is sufficient to induce cardiomyocyte cell cycle reentry. Primary adult rat ventricular cardiomyocytes were stimulated, labeled with BrdU for the last 3 days, and DNA synthesis was determined by immunofluorescence microscopy after 9 days. No stim., no stimulation. NRG1 EGF domain, human NRG1 epidermal growth factor-like domain (amino acids 176–246); NRG1 EC domain, NRG1 extracellular domain (amino acids 1–246).
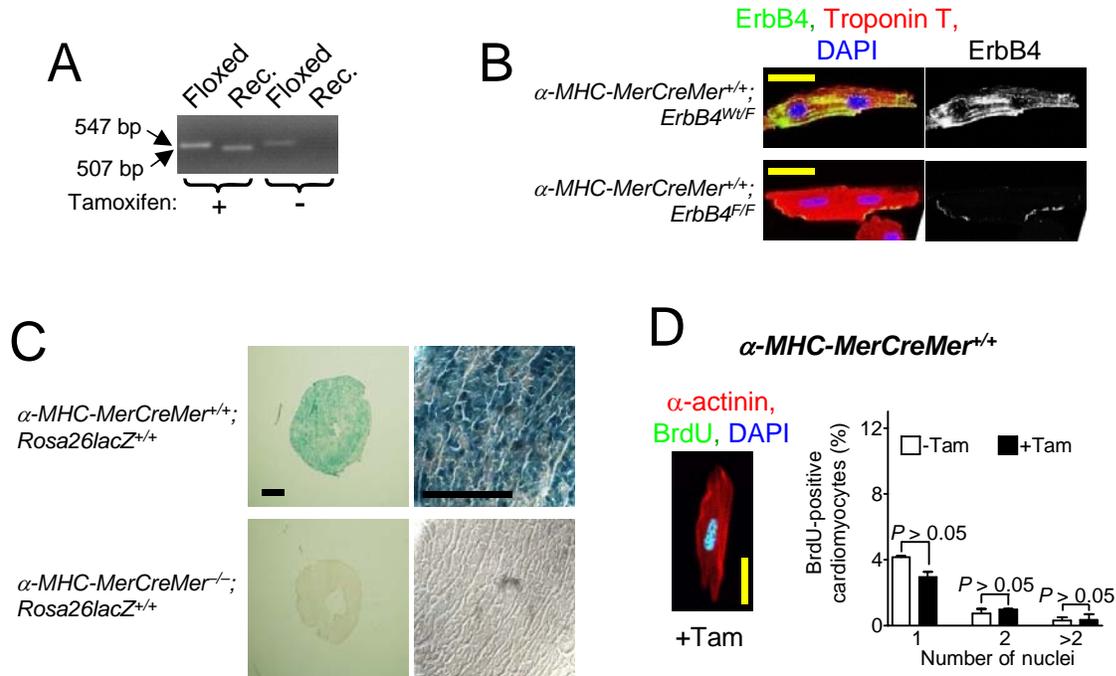
Supplemental Figure and Legend S2

Figure S2. Site-specific recombination in differentiated cardiomyocytes. (A,B) Experiments were performed in α-MHC-MerCreMer^{+/+}; ErbB4[Flox/Flox] (test group) and in α-MHC-MerCreMer^{+/+}; ErbB4[Flox/Wt] (control group) mice. (**A**) PCR on genomic DNA isolated from ventricles of test mice, injected with tamoxifen or with sunflower seed oil. Primer pairs are indicated at the top and were specific for floxed exon 2 of *ErbB4* (Floxed, 547 bp) or for the same locus after site-specific recombination (Rec., 507 bp). (**B**) Reduction of ErbB4 protein levels determined by immunofluorescence microscopy. Scale bars 25 μm. (**C**) Efficiency of site-specific recombination by the α-*MHC-MerCreMer*^{+/+} transgene determined at the *Rosa26lacZ* locus. Mice received tamoxifen injections (100 μg/mg body weight × 5) at 2 weeks of age. Blue X-gal staining, developed 2 weeks later, indicates site-specific recombination, was present in 83.5 ± 2 % of cardiomyocytes (*n* = 7). Scale bars 1 mm (left panels) and 100 μm (right panels). (**D**) Systemic tamoxifen administration does not affect cardiomyocyte cycling in α-*MHC-MerCreMer*^{+/+}; *ErbB4*[Wt/Wt] mice. Statistical significance tested with ANOVA .
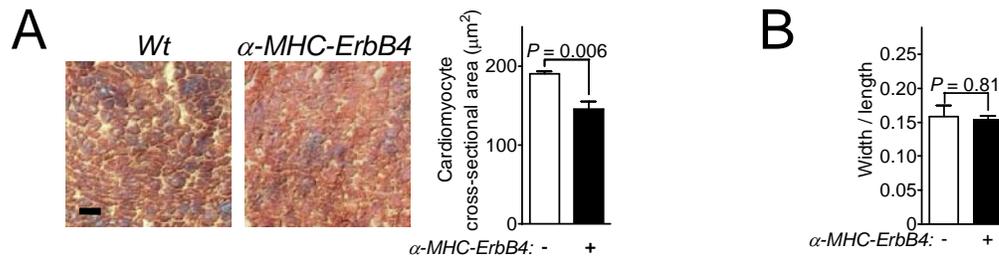
Supplemental Figure and Legend S3

Figure S3. Overexpression of ErbB4 results in smaller cardiomyocytes with normal width/length ratio. (**A,B**) Experiments were performed in α-ErbB4 mice. (**A**) α-MHC-ErbB4 have smaller cardiomyocyte cross-sectional area. (**B**) Smaller cardiomyocytes in α-ErbB4 mice have unchanged width/length ratios. Scale bar 25 μm. Statistical significance tested with t-test.
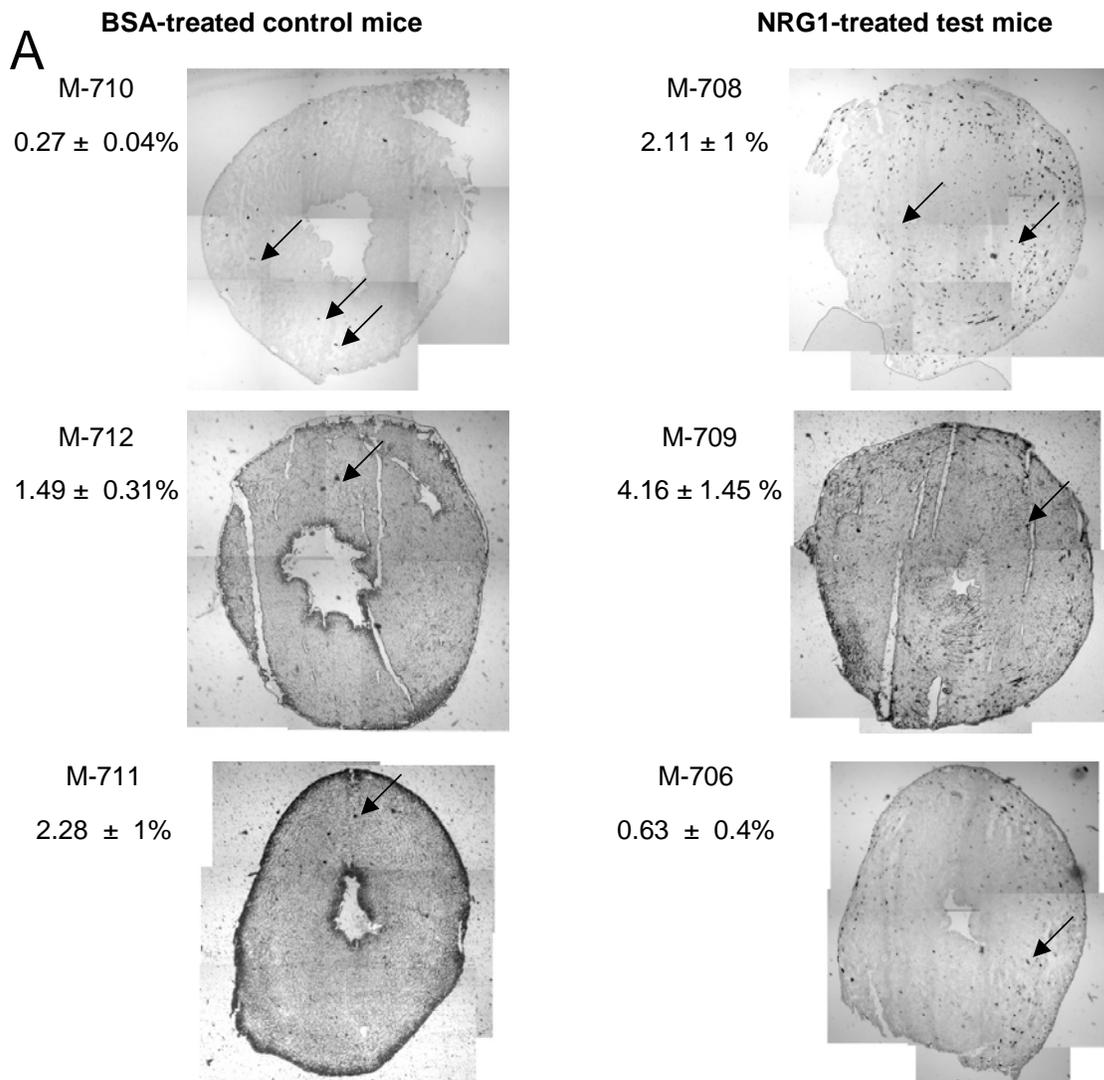
Supplemental Figure and Legend S4

A

BSA-treated control mice   **NRG1-treated test mice**

M-710   M-708

0.27 ± 0.04%   2.11 ± 1 %

M-712   M-709

1.49 ± 0.31%   4.16 ± 1.45 %

M-711   M-706

2.28 ± 1%   0.63 ± 0.4%

Figure S4. Analysis of cardiomyocyte proliferation. α-MHC-MerCreMer$^{+/-}$;Rosa26lacZ$^{+/-}$ were injected with 5 µg/gm tamoxifen once and with NRG1 (2.5 µg/mouse i.p.) for 9 days. (**A**) One representative montaged cross-section from each analyzed heart is shown. Arrow indicates examples of Xgal-positive cardiomyocyte clusters. The recombination rate is given for each heart in mean ± SEM. Large clusters of Xgal-positive cardiomyocytes were not observed.
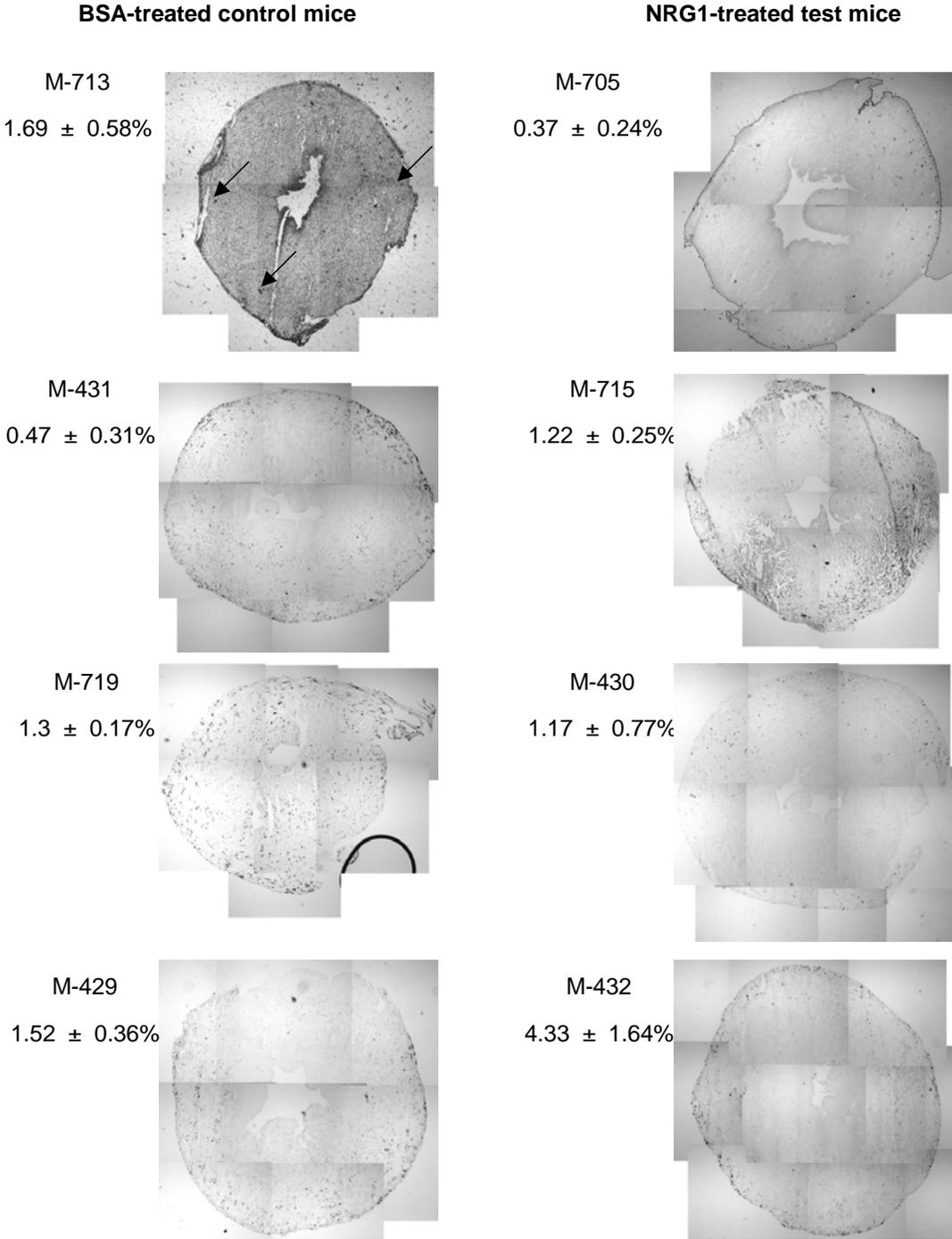
Supplemental Figure and Legend S4, continued

BSA-treated control mice　　　　　　　**NRG1-treated test mice**

M-713

1.69 ± 0.58%

M-705

0.37 ± 0.24%

M-431

0.47 ± 0.31%

M-715

1.22 ± 0.25%

M-719

1.3 ± 0.17%

M-430

1.17 ± 0.77%

M-429

1.52 ± 0.36%

M-432

4.33 ± 1.64%

Figure S4. Analysis of cardiomyocyte proliferation. Continued from previous page.

Supplemental Figure and Legend S4, continued

M-439

0.95 ± 0.29%

M-436

1.18 ± 0.37%

M-437

2.53 ± 0.73%

M-433

1.52 ± 0.59%

B

$P = 0.42$

C

• Clusters of 2 cardiomyocytes
  $r^2 = 0.049$

■ Clusters of ≥ 4 cardiomyocytes
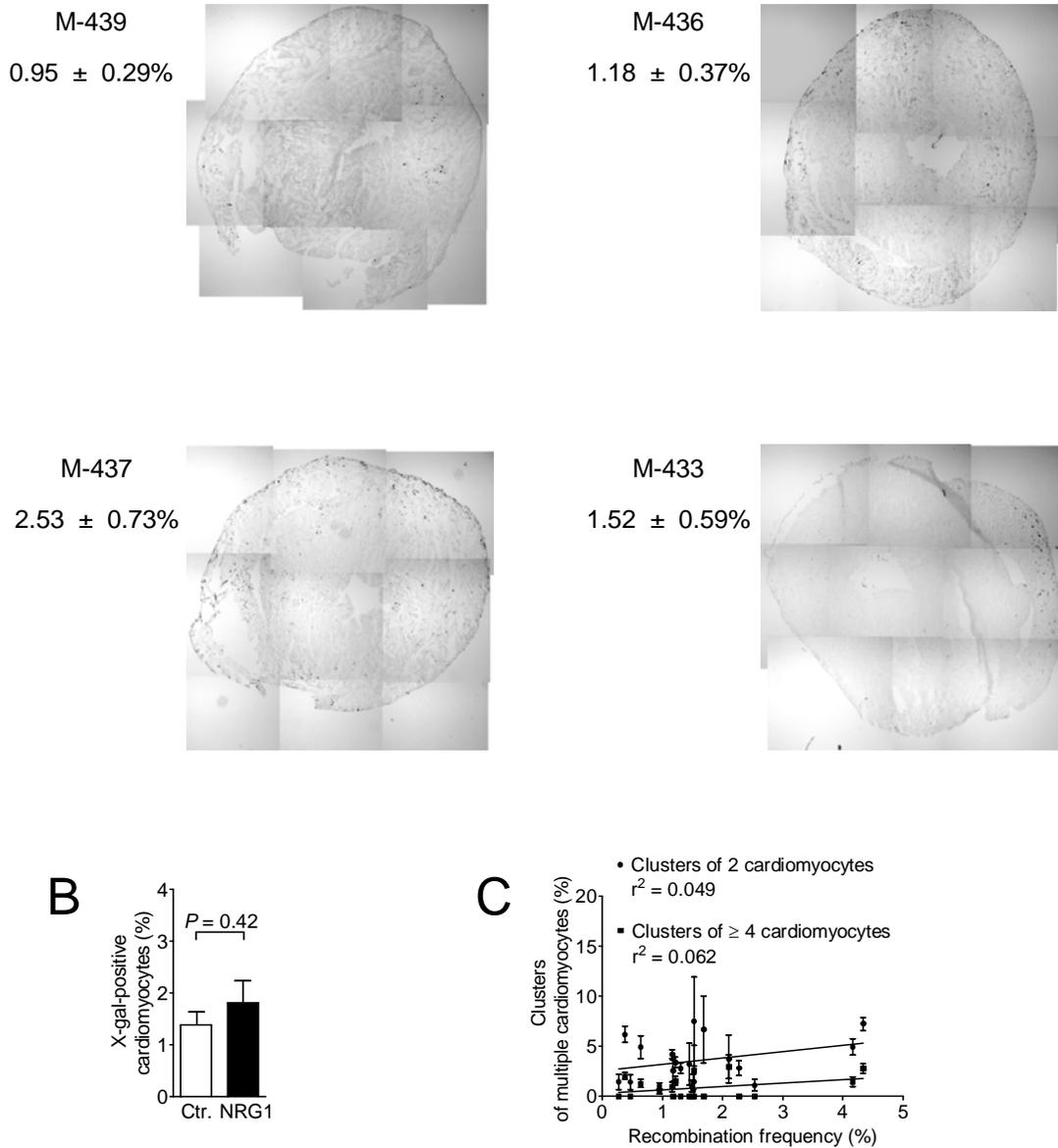 $r^2 = 0.062$

Figure S4. Analysis of cardiomyocyte proliferation. Continued from previous page. (**B**) The percentage of genetically labeled cardiomyocytes was identical in control and NRG1-injected hearts. Statistical significance tested by t-test. (**C**) There was no correlation between the genetic labeling rate and the percentage of labeled bi- and multicellular cardiomyocyte clusters. Goodness of fit (r^2) determined by linear regression.
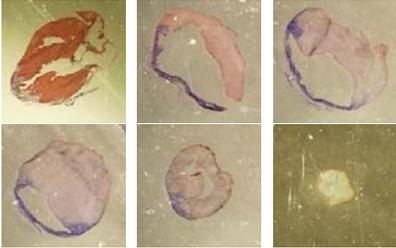
Supplemental Figure and Legend S5
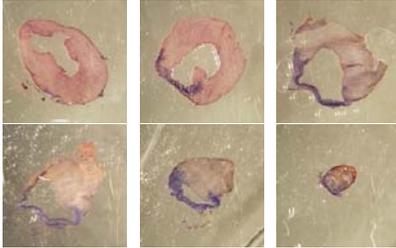
One week treatment after myocardial infarction

BSA-treated control mice   **NRG1-treated test mice**

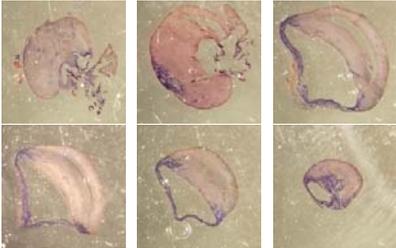MI101   MI105
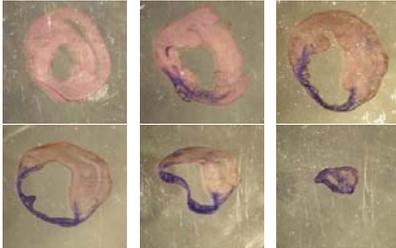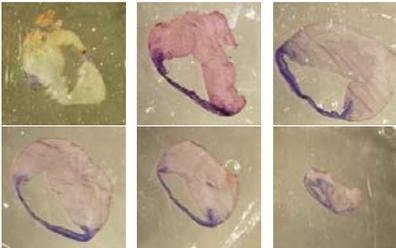

MI103   MI109

MI104   MI110

Figure S5. Visualization of myocardial and scar tissue one week after treatment.

One week treatment after myocardial infarction (continued)

BSA-treated control mice   **NRG1-treated test mice**

MI107   MI111

MI108   MI112

MI113
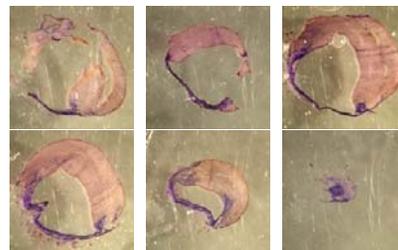
Figure S5. Visualization of myocardial and scar tissue one week after treatment.
Continued from previous page.

Supplemental Figure and Legend S6

Twelve weeks treatment after myocardial infarction

| **BSA-treated control mice** | **NRG1-treated test mice** |

MI125

MI124

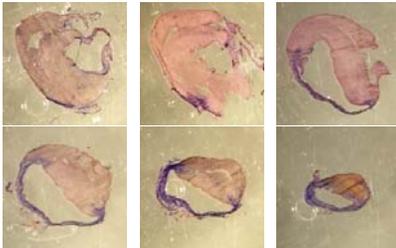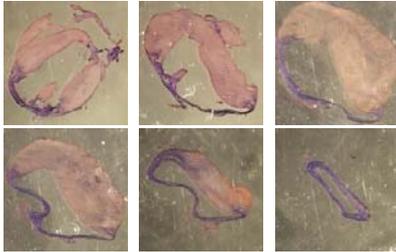MI127

MI126

MI128

MI129
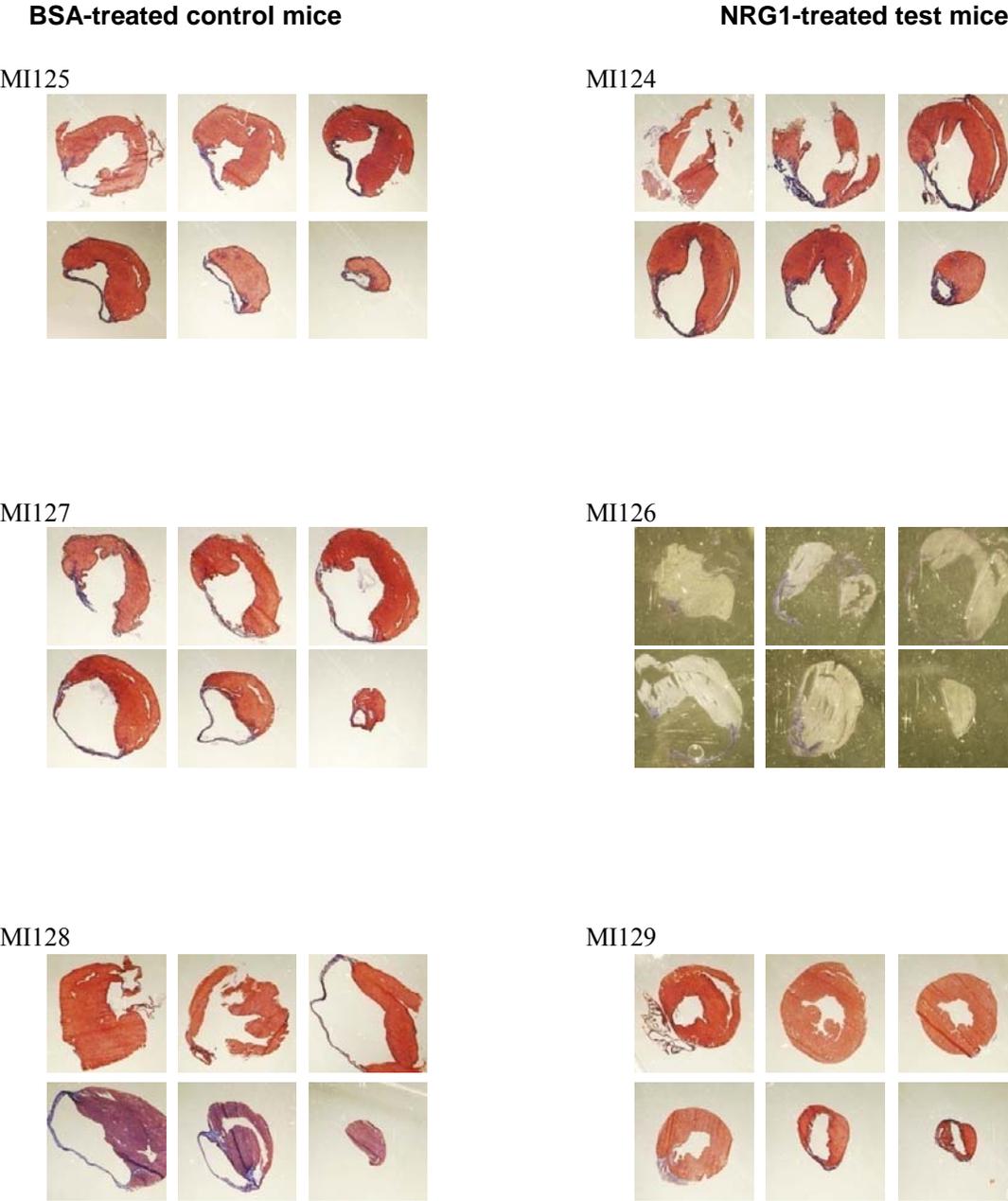
Figure S6. Visualization of myocardial and scar tissue 12 weeks after treatment.

Supplemental Figure and Legend S6, continued

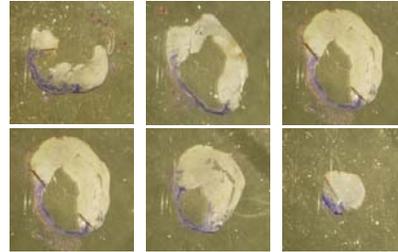**Twelve weeks treatment after myocardial infarction (continued)**

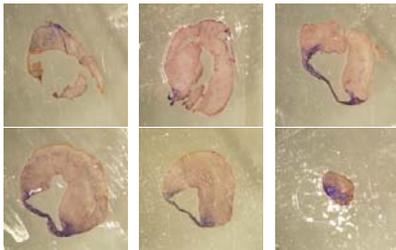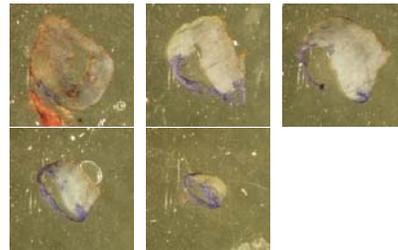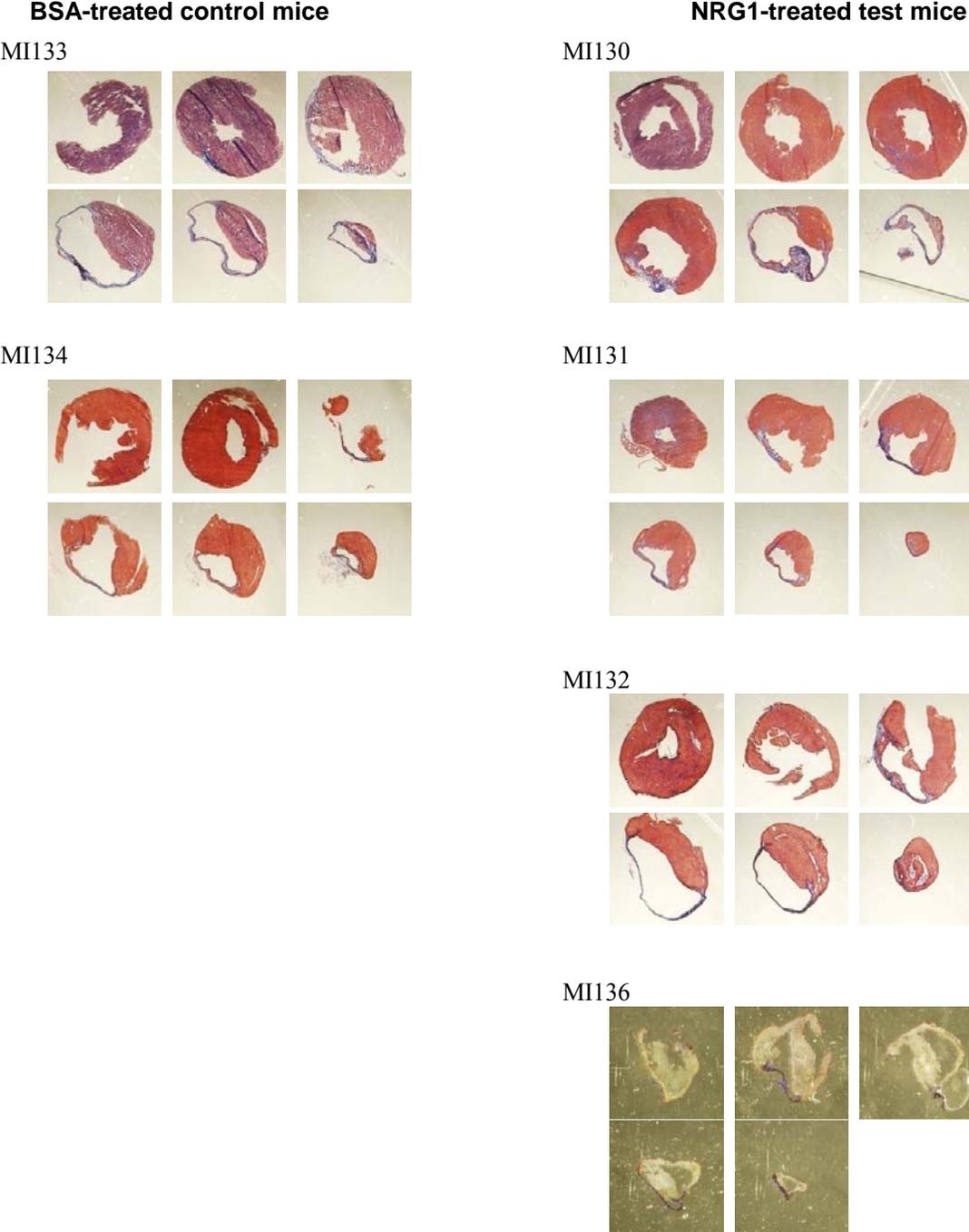| BSA-treated control mice	NRG1-treated test mice

MI133

MI130

MI134

MI131

MI132

MI136

Figure S6. Visualization of myocardial and scar tissue 12 weeks after treatment.
Continued from previous page.

Supplemental Figure and Legend S7

A

c-kit, troponin T, DAPI

- NRG1   + NRG1   Myocardial infarction
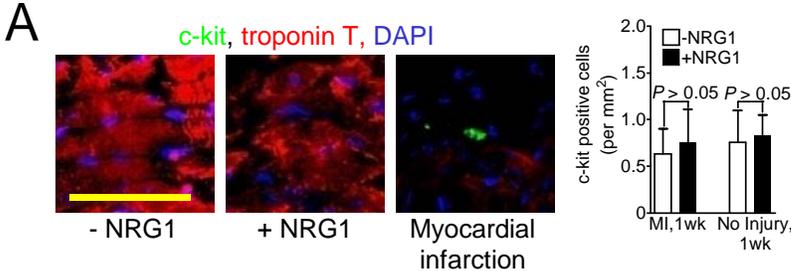
Figure S7. C-kit positive progenitor cells do not contribute to NRG1-induced cardiomyocyte cell cycle activity. NRG1 does not induce recruitment of c-kit positive progenitor cells to the myocardium. Color codes indicated at the top. Scale bars, 50 μm. Statistical significance was determined by ANOVA.

Supplemental Tables

Table S1. Characterization of effect of *ErbB4* inactivation on cardiomyocyte proliferation and myocardial function and structure.

|	*ErbB4$^{Wt/F}$*	*ErbB4$^{F/F}$*	Statistical significance
Histology:			
n	9	6	
Body weight (gm)	6.8 ± 0.4	8.5 ± 0.6	*P* > 0.05
Heart weight (mg)	49.6 ± 2.7	58.2 ± 4.8	*P* > 0.05
Heart/body weight (mg/gm)	7.3 ± 0.2	6.8 ± 0.2	*P* > 0.05
Tissue density of cardiomyocyte nuclei (mm^{-3})	58,630 ± 1,546	47,340 ± 2,500	*P* < 0.05
Echocardiography:			
n	8	6	
Contractility (FS, %)	48.5± 3.0	47.9 ± 2.1	*P* > 0.05
Interventricular septum in diastole (mm)	0.7 ± 0.04	0.7 ± 0.03	*P* > 0.05
Left ventricular internal dimension in diastole (mm)	2.3 ± 0.1	2.0 ± 0.4	*P* > 0.05

Legend to Table S1. Morphometric and histologic analyses were performed on resected hearts at 19 days of age. Echocardiography was performed with a 40 MHz probe and images were recorded and analyzed with a Visualsonics ultrasound machine. Data are mean ± SEM. Statistical significance was tested by ANOVA (Bonferroni method).

Table S2. Morphometric characterization of α-MHC-ErbB4 transgenic mice.

Age	2 weeks		
	Control	**α-MHC-ErbB4 transgene**	**Statistical significance**
n	5	6	
Tissue density of cardiomyocyte nuclei (mm^{-3})	75,520 ± 4,435	90,720 ± 3,375	*P* < 0.001
LV myocardial volume (mm^3)	24.5 ± 1.0	22.4 ± 1.5	*P* > 0.05
Cardiomyocyte volume (μm^{-3})	9,429 ± 3,217	8,166 ± 2,978	*P* = 0.0009
Cardiomyocyte cross-sectional area (μm^2)	191 ± 3	146 ± 10	*P* = 0.0062

Legend to Table S2. Morphometric and histologic analyses were performed on resected hearts at 15 days of age. Data are mean ± SEM. Statistical significance was tested by ANOVA (Bonferroni method) and t-test (cardiomyocyte volume and cross-sectional area).

Table S3. Biometric data of *α-MHC-ErbB4* transgenic mice.

Age	2 weeks			2 months		
	Control	***α-MHC-ErbB4* transgene**	**Statistical significance**	**Control**	***α-MHC-ErbB4* transgene**	**Statistical significance**
n	5	6		6	6	
Body weight (gm)	7.7 ± 0.2	7.3 ± 0.2	$P > 0.05$	$19.0. \pm 0.5$	20.4 ± 1.2	$P > 0.05$
Heart weight (mg)	52.4 ± 2.1	51.5 ± 1.6	$P > 0.05$	108.1 ± 1.9	109.8 ± 4.9	$P > 0.05$
Heart/body weight (mg/gm)	6.8 ± 0.2	7 ± 0.1	$P > 0.05$	5.4 ± 0.1	5.7 ± 0.1	$P > 0.05$

Legend to Table S3. Biometric analyses were performed on resected hearts at 15 days of age. Data are mean ± SEM. Statistical significance was tested by ANOVA (Bonferroni method).

Table S4. Functional characterization of *α-MHC-ErbB4* transgenic mice.

Age	2 weeks			2 months		
	Control	***α-MHC-ErbB4* transgene**	**Statistical significance**	**Control**	***α-MHC-ErbB4* transgene**	**Statistical significance**
n	6	10		6	6	
Contractility (FS, %)	51.1 ± 3.5	48.6 ± 2.2	$P > 0.05$	52.1 ± 2.1	51.8 ± 1.5	$P > 0.05$
Interventricular septum in diastole (mm)	0.7 ± 0.1	0.6 ± 0.05	$P > 0.05$	0.8 ± 0.1	0.8 ± 0.3	$P > 0.05$
Left ventricular internal dimension in diastole (mm)	2.4 ± 0.2	2.5 ± 0.1	$P > 0.05$	4.0 ± 0.1	4.1 ± 0.1	$P > 0.05$

Legend to Table S4. Echocardiography was performed with a 10 MHz probe and images were recorded and analyzed with a Vivid *i* ultrasound machine. Data are mean ± SEM. Statistical significance was tested by ANOVA (Bonferroni method).

Table S5. Functional and structural effects of NRG1 treatment after myocardial infarction determined by echocardiography.

	Ctr.						NRG1					
Time after start of treatment (weeks)	0	1	4	8	12	14	0	1	4	8	12	14
n	23	7	15	14	13	12	23	7	15	15	14	14
$LVID_d$ (mm)	4.91 ± 0.13	5.24 ± 0.14	5.24 ± 0.10	5.60 ± 0.16	5.83 ± 0.12*	5.80 ± 0.16*	4.95 ± 0.10	5.50 ± 0.14	5.15 ± 0.11	5.22 ± 0.17	5.30 ± 0.13*	5.31 ± 0.13*
$LVID_s$ (mm)	4.18 ± 0.13	4.41 ± 0.17	4.63 ± 0.09	4.89 ± 0.18	5.15 ± 0.10*	5.21 ± 0.18*	4.15 ± 0.12	4.68 ± 0.10	4.27 ± 0.12	4.24 ± 0.18	4.48 ± 0.16*	4.53 ± 0.14*
EF (%)	32.23 ± 1.579	33.18 ± 2.15	25.94 ± 1.03***	27.2 ± 2.01***	22.34 ± 1.07**	21.85 ± 1.24**	33.99 ± 2.17	31.02 ± 1.18	35.55 ± 1.48***	39.01 ± 1.89***	32.69 ± 2.23**	31.39 ± 1.36**
IVS_d (mm)	0.75 ± 0.03	0.83 ± 0.08	0.73 ± 0.03	0.66 ± 0.04	0.62 ± 0.03*	0.60 ± 0.04*	0.83 ± 0.04	0.62 ± 0.04	0.74 ± 0.03	0.79 ± 0.03	0.77 ± 0.04*	0.79 ± 0.04*
$LVPW_d$ (mm)	0.89 ± 0.03	0.82 ± 0.04	0.75 ± 0.03	0.83 ± 0.04	0.76 ± 0.04	0.72 ± 0.02	0.90 ± 0.03	0.84 ± 0.04	0.85 ± 0.04	0.87 ± 0.04	0.80 ± 0.03	0.78 ± 0.04

Legend to Table S5. Echocardiography was performed with a 40 MHz probe and images were recorded and analyzed with a Visualsonics ultrasound machine. In the control group, two animals died spontaneously and one during anesthesia and in the NRG1-group one animal was removed due to overgrowth of the upper incisors. Statistical significance was tested by ANOVA (Bonferroni method). * $P < 0.05$, ** $P < 0.01$, *** $P < 0.001$

Table S6. Cardiomyocyte proliferative indices of selected vertebrates.

Species	Newt (Notophthalmus viridescens)[1], *in vitro*	Zebrafish (Danio rerio), *in vivo*[2]	Rat (Wistar, this report), *in vitro*	Mouse (C57, this report), *in vivo*
Age of animals	Adult	Adult (100 mg)	3 months (250–300 gm)	2–3 months (20–25 gm)
Mitogen added	10% fetal bovine serum	Endogenous	Neuregulin 1 (100 ng/mL)	Neuregulin 1 (2.5 μg/mouse i.p.)
Mononucleated fraction (%)	>98%	95.1%	11.2%	~10%
DNA synth. (%) Label time	75% At 18 days in culture ^{3}H-thymidine $\times$ 15 days	10.1% Daily BrdU $\times$ 3 days	0.4–1% At 9 days in culture BrdU $\times$ 3 days	0.9% 9 days continuous BrdU
Karyokinesis (%)	1.2% (phosphorylated histone H3) 60% (cumulative over 18 days)	ND	3% (metaphase plate cumulative over 6 days)	0.4% (instantaneous, of mononucleated)
Cytokinesis (abscission, %)	29% (cumulative over 18 days)	ND	0.6% (cumulative over 6 days)	0.25% (instantaneous, of mononucleated)

Legend to Table S6. [1] Bettencourt-Dias, M., Mittnacht, S. & Brockes, J.P. Heterogeneous proliferative potential in regenerative adult newt cardiomyocytes. *J Cell Sci* **116**, 4001-4009 (2003). [2] Wills, A.A., Holdway, J.E., Major, R.J & Poss, K.D. Regulated addition of new myocardial and epicardial cells fosters homeostatic cardiac growth and maintenance in adult zebrafish. *Development* **135**, 183-192 (2008).

Table S7. Image acquisition.

	Acquisition Settings	
	Hardware	**Software and settings**
Fig. 1E,F,H	Olympus IX-81 epifluorescence microscope[1] with UPLFL ×10, NA 0.3 (phase contrast micrographs) and LUCPLFL ×40, NA 0.6 (immunofluorescence micrographs) lenses and equipped with Hamamatsu EM CCD C9100	10–100 msec exposure, 12 bit, IP lab 4[3]
Fig. 1I	Olympus IX-81 microscope[1] with LucPlanFLN ×20 lens, NA 0.45, illuminated with a 100 W mercury arc lamp	Phase: 10 msec exposure, EGFP-fluorescence: 1,200 msec exposure, 12 bit, IP lab 4[3]
Fig. 2B,G	Olympus FV 1000 laser scanning confocal microscope[1] with ×60 S-Achromat lens, confocal aperture 125 μm	Fluoview software[1] Vers. 1.4a, 2 sec/px, zoom 2, 1,024×1,024 px, Argon laser for 488 nm, He/Ne laser for 594 nm
Fig. 2D	Olympus IX-81 epifluorescence microscope[1] with UPLFL ×10, NA 0.3 (phase contrast micrographs) and LUCPLFL ×40, NA 0.6 (immunofluorescence micrographs) lenses and equipped with Hamamatsu EM CCD C9100	10–100 msec exposure, 12 bit, IP lab 4[3]
Fig. 3D	Olympus DSU spinning disk confocal microscope[1] with ×60 UPlanSApo, 1.2 NA lens; equipped with Hamamatsu EM CCD C9100	200–300 msec exposure, Slidebook[1]
Fig. 3E	Olympus FV 1000 laser scanning confocal microscope[1] with ×60 S-Achromat lens, confocal aperture 125 μm	Fluoview software[1] Vers. 1.4a, 2 sec/px, zoom 2, 1,024×1,024 px, Argon laser for 488 nm, He/Ne laser for 594 nm
Fig. 4B,C,K,L	Olympus DSU spinning disk confocal microscope[1] with ×60 UPlanSApo, 1.2 NA lens; equipped with Hamamatsu EM CCD C9100	200–300 msec exposure, Slidebook[1]
Fig. 4D	Axioplan 2 Epifluorescence microscope[2], PlanNeofluar ×40 lens, NA 0.6	Axiocam[2], Axiovision[2], 200-600 msec exposure, 1,300x1,300 px, 8 bit

| | **Acquisition Settings** | |
	Hardware	Software and settings
Fig. 4G-I	Olympus IX-81 epifluorescence microscope[1] with UPLFL ×10, NA 0.3 (phase contrast micrographs) and LUCPLFL ×40, NA 0.6 (immunofluorescence micrographs) lenses and equipped with Hamamatsu EM CCD C9100	10–100 msec exposure, 12 bit, IP lab 4[3]
Fig. 5A,B	Olympus DSU spinning disk confocal microscope[1] with ×60 UPlanSApo, 1.2 NA lens; equipped with Hamamatsu EM CCD C9100	200–300 msec exposure, Slidebook[1]
Fig. 6C Fig. 6F	Nikon SMZ 1000 dissecting microscope[4] equipped with Olympus DP70 Olympus IX-81 epifluorescence microscope[1] with UPLFL ×10, NA 0.3 (phase contrast micrographs) and LUCPLFL ×40, NA 0.6 (immunofluorescence micrographs) lenses and equipped with Hamamatsu EM CCD C9100	13 sec exposure, 680 × 512 px, Olympus DP controller[1] 10–100 msec exposure, 12 bit, IP lab 4[3]
Fig. 7A,D,E,G	Olympus DSU spinning disk confocal microscope[1] with ×60 UPlanSApo, 1.2 NA lens; equipped with Hamamatsu EM CCD C9100	200–300 msec exposure, Slidebook[1]

Legend to Table S7. Key to manufacturers: [1] Olympus America Inc. Melville, NY; [2] Carl Zeiss Inc., Thornwood, NY; [3] BD Biosciences Bioimaging. Rockville, MD, [4] Nikon Instruments Inc., Melville, NY.

Table S8. Quantification of numeric data.

Figure	Assay	Number of cardiomyocytes, nuclei, and hearts analyzed
Fig. 1E	BrdU uptake	68,913 cardiomyocytes derived from 6 different hearts
Fig. 1F	Contractile ring formation	83,623 cardiomyocytes derived from 7 different hearts
Fig. 2A,B	DAPI/BrdU uptake	2,124 cardiomyocytes from 8 different hearts
Fig. 2D,E	DAPI/BrdU uptake	4,285 cardiomyocytes from 11 different hearts
Fig. 2F	Apoptotic cardiomyocytes	1 section from 14 different hearts
Fig. 2G	Volume density of cardiomyocyte nuclei	3 sections per heart from 11 different hearts
Fig. 2H	Cardiomyocyte volume	353 cardiomyocytes from 8 different hearts
Fig. 3B,C	BrdU uptake, Mono/multinucleated	32,366 cardiomyocytes from 12 different hearts
Fig. 3D	Karyokinesis	20,501 cardiomyocytes from 7 different hearts
Fig. 3E	Cytokinesis	5 sections/heart from 5 different hearts
Fig. 4E	Clonal analysis *in vivo*	4,378 clones from 10 control and 9 NRG1-injected hearts
Fig. 4J	CldU/IdU uptake	14,028 cardiomyocytes from 4 NRG1-stimulated and 3 control hearts
Fig. 5D,E	Dynamic genetic fate map	49,915 cardiomyocytes from 11 different hearts
Fig. 6B	Echocardiography	Data collected in triplicates from 32 animals at each time point
Fig. 6D	Scar size	Data collected from 23 hearts
Fig. 6E	Heart weight / tibia length	Biometric data collected from 32 animals
Fig. 6F	Cross-sectional area	3 sections/heart from 10 hearts

Fig. 7A	BrdU uptake	3 sections/heart from 21 hearts
Fig. 7B	Apoptosis	1 section/heart from 24 hearts
Fig. 7C,H	Mono/multinucleated, BrdU uptake	171,212 cardiomyocytes from 6 NRG1-stimulated and 5 control hearts
Fig. 7D	Karyokinesis	3 sections/heart from 11 hearts
Fig. 7E	Cytokinesis	3 sections/heart from 11 hearts
Fig. 7F	Cardiomyocyte nuclei	3 sections/heart from 21 hearts

Supplemental References

Golub, M. S., Germann, S. L., and Lloyd, K. C. (2004). Behavioral characteristics of a nervous system-specific erbB4 knock-out mouse. Behav Brain Res *153*, 159-170.

Howard, C. V., and Reed, M. (2005). Unbiased Stereology: Three-Dimensional Measurement In Microscopy, 2nd edn (Oxford: BIOS Scientific Publishers).

Jackson-Fisher, A. J., Bellinger, G., Shum, E., Duong, J. K., Perkins, A. S., Gassmann, M., Muller, W., Kent Lloyd, K. C., and Stern, D. F. (2006). Formation of Neu/ErbB2-induced mammary tumors is unaffected by loss of ErbB4. Oncogene *25*, 5664-5672.

Kuhn, B., Del Monte, F., Hajjar, R. J., Chang, Y. S., Lebeche, D., Arab, S., and Keating, M. T. (2007). Periostin induces proliferation of differentiated cardiomyocytes and promotes cardiac repair. Nat Med *13*, 962-969.

Sohal, D. S., Nghiem, M., Crackower, M. A., Witt, S. A., Kimball, T. R., Tymitz, K. M., Penninger, J. M., and Molkentin, J. D. (2001). Temporally regulated and tissue-specific gene manipulations in the adult and embryonic heart using a tamoxifen-inducible Cre protein. Circ Res *89*, 20-25.

Soriano, P. (1999). Generalized lacZ expression with the ROSA26 Cre reporter strain. Nat Genet *21*, 70-71.

Tidcombe, H., Jackson-Fisher, A., Mathers, K., Stern, D. F., Gassmann, M., and Golding, J. P. (2003). Neural and mammary gland defects in ErbB4 knockout mice genetically rescued from embryonic lethality. Proc Natl Acad Sci U S A *100*, 8281-8286.